Macroscopic Electrical Properties of Ordered Single-Walled Carbon Nanotube Networks

Pornnipa Vichchulada, Qinghui Zhang, Alicia Duncan, and Marcus D. Lay*

Department of Chemistry and NanoScale Science and Engineering Center (NanoSEC), University of Georgia, Athens, Georgia 30602

ABSTRACT Creation of large-scale arrays of single-walled carbon nanotubes (SWNTs) with defined orientation and density is of central importance for obtaining functional electronic device structures that incorporate these nanoscaled systems. This manuscript describes how the macroscopic electrical properties of 2D SWNT networks vary controllably with the microscopic alignment individual SWNTs in the network. These studies indicate that "orthogonal" SWNT structures provide enhanced reproducibility and conductivity, when compared to deposits of highly aligned SWNTs. Because this material is composed of a submonolayer coverage of SWNTs, such deposits have applications in flexible and transparent electronic materials.

KEYWORDS: carbon nanotube • SWNT • crossbar • aligned CNTs • array • nanowire • room-temperature deposition

INTRODUCTION

Single-walled carbon nanotubes (SWNTs) have attracted much interest because of their enhanced physical and electrical properties; they have the highest known tensile strength, are compatible with flexible substrates, and can act as either semiconductors or metallic conductors (1−6). SWNTs have shown promise in technologies as diverse as high-performance nanoscaled transistors (7−10), electrical interconnects (11−14), flexible electronic materials (15−17), electrochemical (18−21) and gas sensors (22−25). Further, unlike indium tin oxide (ITO), polycrystalline Si, or Si nanowires, 2D SWNT networks are uniquely suitable for flexible electronic applications, as SWNTs bend to conform to flexible substrates and their electronic properties vary little upon bending (6, 26−29).

For the aforementioned applications to reach fruition, methods for the controlled deposition of SWNT networks, with controlled density and orientation, must be developed (30, 31). Chemical vapor phase deposition (CVD) is a common technique used to grow aligned SWNT mats or networks (32). However, this high-temperature growth process occurs at temperatures that preclude the use of many industrially relevant substrates (such as polymers and glass). The laminar flow deposition (LFD) technique under development in this research group has the advantage of decoupling the growth process (which occurs ~800 °C) from the deposition process (which occurs at room temperature), allowing the formation of SWNT networks of arbitrary density on numerous substrates via repeated deposition cycles that each deposit a reproducible density of SWNTs (33−35). The results herein demonstrate the reproducibility of the LFD technique for formation of partially aligned 2D thin films of SWNTs; the macroscopic electronic properties

of these networks have anisotropic electronic transport, strongly affected by the alignment direction of the substrate with respect to the deposition direction during thin-film growth.

EXPERIMENTAL METHODS

SWNT Suspension Preparation. Twenty-five milliliters of an aqueous suspension of 1 mg/mL AP-grade SWNT arc discharge soot (Carbolex) in 1 % (w/v) sodium dodecyl sulfate (J.T. Baker) was prepared via probe sonication (Fisher, Model 500) for 30 min at 12 W. Purification involved multiple centrifugation cycles (Beckman, GS-15R) at 18,000 G for 45 min./cycle, followed by removal of the upper half of the supernatant from the centrifuge tube. The centrifugation/decantation process was repeated three times. Bundles of SWNTs, amorphous carbon (formed during the growth process) and metal catalyst nanoparticles were removed in the sediment during the centrifugation process. This purification method has proven successful in formation of suspensions of unbundled, long, pristine SWNTs (36).

Deposition of SWNTs through Laminar Flow Deposition. The substrates for all 2D network growth were Si/SiO_x wafer fragments, with a thermally grown 500 nm silicon oxide dielectric layer. This surface was cleaned with a CO_2 snow-jet and then modified with a monolayer of 3-aminopropyl-triethoxy-silane (35). The silane was used to adhere the SWNTs to the surface of the Si/SiO_x wafer fragment. "Aligned" and "orthogonal" arrays were fabricated using a liquid deposition technique under development in this group, which avoids bundle formation during the SWNT deposition procedure (33, 34). Briefly, the surface was wet with 100 μL of SWNT suspension. Next, high-purity N_2 flow at 60 psi was used to effect laminar drying of the solution in one direction, resulting in arrays of SWNTs aligned in the drying direction. Laminar flow was observed during drying if the stream of N_2 had a contact angle of between 30 and 45°. Following each SWNT deposition cycle, the substrate was rinsed with copious amounts of nanopure water.

Each deposition cycle results in the deposition of a reproducible density of SWNTs on the substrate. Previously published work has shown that the density of SWNTs on the surface increased at a rate of 0.37 SWNTs/μm^2 for deposits formed from suspensions with the same starting concentration as those used in these studies (37). In fact, the SWNT density, as observed from atomic force microscopy (AFM) images, increased at a constant rate for the first eight deposition cycles (Figure 1).
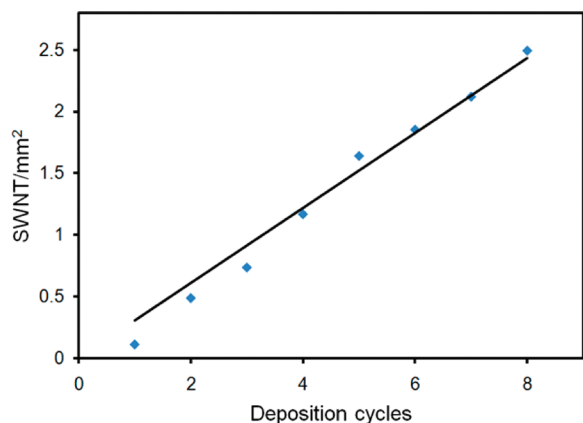
FIGURE 1. For SWNTs aligned in one direction, the density of SWNTs observed increases at a rate of 0.37 SWNT/μm^2 per deposition cycle. This deposition rate is constant over repeated deposition cycles.
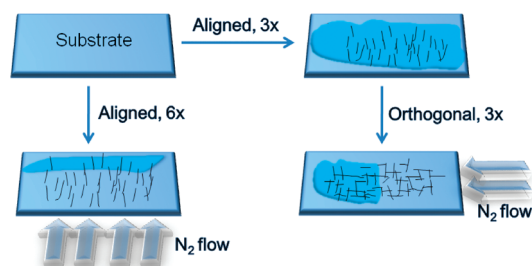

FIGURE 2. Laminar flow deposition (LFD) was used to form two types of macroscopic SWNT networks; "aligned" networks were formed from six successive deposition cycles, whereas "orthogonal" networks were formed from three deposition cycles in one direction, followed by three more at an orthogonal angle.

For the work presented herein, six consecutive deposition cycles were used to create the "aligned" networks of SWNTs (Figure 2). Though the SWNTs are largely aligned, the errant nanotubes are likely responsible for much of the current carrying ability of these networks of aligned SWNTs, as they provide local electrical pathways between highly aligned SWNTs. Without these errant SWNTs, macroscopic conductivity would depend entirely on end-to-end registry of SWNTs, and a much higher loading of SWNTs would be needed.

To achieve SWNT "orthogonal" assemblies, three successive deposition cycles, designed to align the SWNTs in one direction, were followed by three more with orthogonal directionality. This method of SWNT network deposition resulted in a more homogeneous distribution of the orientations of SWNTs. In these "orthogonal" deposits, there are many more inter-SWNT junctions, as the SWNTs have a more random orientation. This type of network is expected to yield the highest macroscopic conductivity with the lowest loading of SWNTs.

The ability of the LFD method to deposit a reproducible number of SWNTs per deposition cycle allows the formation of macroscopic networks of SWNTs that are similar in density, yet differ in the overall alignment of the SWNTs. Therefore, the differences in resistance for the two types of networks studied can be ascribed to the number of inter-SWNT junctions, with "orthogonal" networks having a significantly greater number of such junctions than "aligned" networks.

Characterization Methods. The purity of SWNT suspensions were verified using UV–vis and Raman spectroscopy. UV–vis spectroscopy (Varian, Carey 300) was performed in a liquid cell with a path length of 1 cm. For Raman spectroscopy (Thermo Scientific, DXR Raman Microscope), a 532 nm diode laser with an intensity of 10mW measured at the sample was used for excitation. Each spectrum took 60 s to record with a CCD
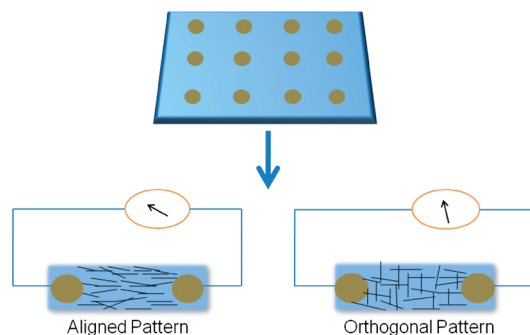

FIGURE 3. Schematic of the types of electrical measurements made for "aligned" and "orthogonal" patterns of SWNTs networks. The distance between electrodes was 0.5 cm.
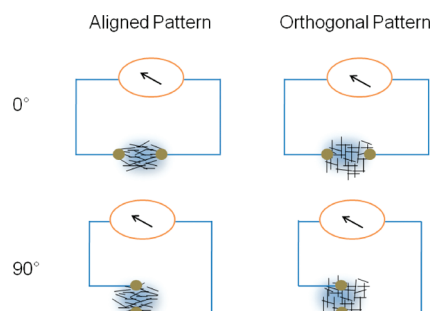

FIGURE 4. Electrical resistance was measured in two directions, 0 and 90°, with respect to the initial SWNT deposition direction for each pattern in order to determine the effect of SWNT alignment on macroscopic conductivity.

detector. Deposit morphology and alignment was ascertained by analysis of AFM (Molecular Imaging, PicoPlus) images using SPIP v. 5.04 (ImageMetrology). A semiconductor characterization system (Keithley, 4200SCS) and probe station (Signatone, S-1160A) were used for macroscopic electrical measurements. Since four-point-probe and two-point probe measurements of conductivity yielded statistically insignificant differences in values, two-point probe measurements were performed to characterize the macroscopic electronic properties of these thin films by depositing 0.2 cm diameter electrodes with the spacing of 0.5 cm using a stencil mask and silver paint (Figure 3). Similar two-point probe studies have proven effective for the study of SWNT networks in previously published work (38, 39). For each SWNT pattern, the electrical resistance was measured in two directions: 0 and 90° with respect to the initial SWNT deposition direction (Figure 4). The resistance was calculated on the basis of the average R for each device, obtained at 50 points during a potential scan from -1 to $+1$ V.

RESULTS AND DISCUSSION

UV–Vis and Raman Spectroscopy Analysis of SWNT Suspensions. Deposition suspensions were prepared using multiple centrifugation cycles at low G (36). Prior to network deposition, each aqueous SWNT suspension was examined with UV–vis spectroscopy to verify the existence of individual, debundled SWNTs (Figure 5a). Before purification, SWNT suspensions exhibited a broad, featureless absorbance band. After purification, the presence of the first interband transitions for metallic (M_{11}, 580 nm) and semiconductive (S_{22}, 730 nm) SWNTs in the UV–vis spectra indicates the presence of a suspension enriched in individual SWNTs (40, 41).

The removal of amorphous carbon impurities was also verified with Raman spectroscopy (Figure 5b). Raman spec-
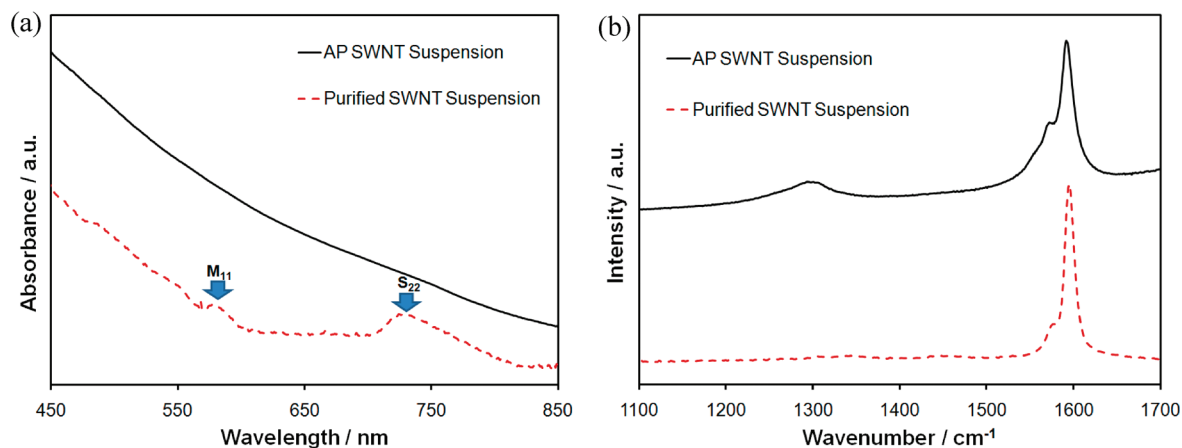
FIGURE 5. Optical spectroscopy of suspensions of long, unbundled SWNTs: (a) UV−vis spectrum showing increase in peaks for the M_{11} and S_{22} electronic transitions; (b) Raman spectroscopy shows the G-band at 1591 cm^{-1} for the pristine symmetrical graphene lattice.
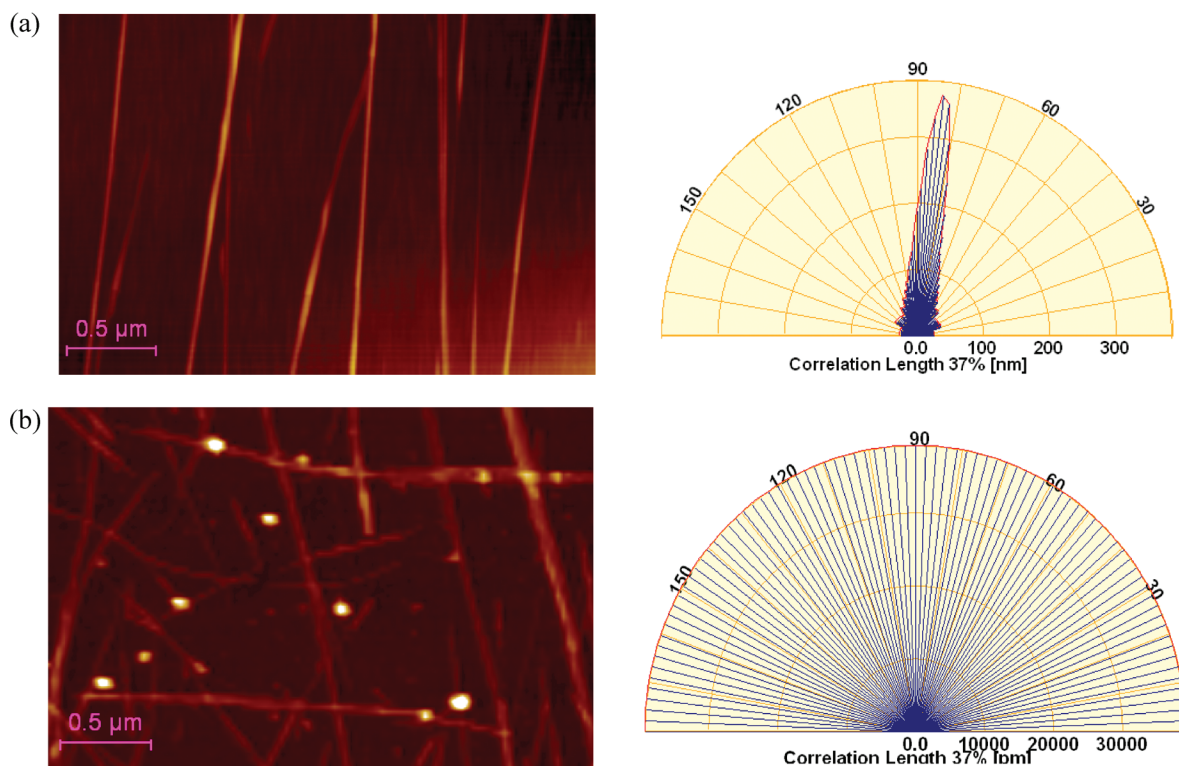

FIGURE 6. Topographic AFM images and autocorrelation graphs for the two types of SWNT deposits investigated: (a) for the "aligned" deposit, the AFM image and autocorrelation graph shows a significant level of alignment in the SWNTs; (b) for the "orthogonal" deposit, the AFM image and autocorrelation graph indicates no single alignment direction.

tra obtained after purification showed a greatly reduced disorder-induced band (D-band) in the range 1300−1370 cm^{-1}. The D-band is caused by the scattering of asymmetrical sp^2 bonds in the C lattice (42, 43). These types of bonds are indicative of anomalies like C-atom vacancies, or oxidative defect sites. The graphite band (G-band), observed at 1591 cm^{-1}, signifies the pristine symmetrical graphene lattice (44, 45). As pristine SWNTs are composed entirely symmetrical sp^2 bonds, a reduction in the D-band indicates removal of the carbonaceous impurities formed during SWNT growth, leaving the suspensions of long undamaged SWNTs used in these studies.

AFM Analysis of Aligned SWNT Arrays. Topographic AFM images of each deposit were analyzed to ascertain the level of alignment obtained. When the Str 37 function in AFM image analysis software SPIP was used to quantitate the level of alignment for the two types of samples, significant differences were observed between the aligned and orthogonal samples (Figure 6). This function defines a series of high areas on the surface as autocorrelation centers and an autocorrelation function is employed to the z-range data in all directions away from these centers. Then, the ratio of the height (or z-range) for each pixel to the distance away from the autocorrelation center is calculated in all directions from the autocorrelation center. Next, Str 37 is defined as the boundary at which this ratio decays to 37 % of the z-range at the autocorrelation center. The quantity 37 % is chosen so the natural logarithm of the height

difference between each center and its boundary is unity, as the natural logarithm is used in the Fourier transform of the image. This decay in z-range in all directions from each autocorrelation center is then evaluated in the calculation of Str 37 for each image, allowing quantitation of the degree, as well as direction, of alignment for SWNT arrays.

To understand this function from an empirical perspective: a slow decay, corresponding to a relatively long correlation length (on the x-aixs of the Str histogram) is found as one traverses a nanotube along its axis. Meanwhile, a fast decay is observed as one traverses a nanotube orthogonal to its axis. In an image containing multiple SWNTs, the ratio between these two decay functions is determined for each autocorrelation center and averaged for the entire image. Therefore, for a series of highly aligned SWNTs, the Str 37 histogram will show a high density of observations in the direction of alignment of SWNTs and very few observations in other directions (Figure 6a). However, the Str 37 histogram for a network composed of SWNTs with roughly half oriented in one direction and half in an orthogonal direction will show no major axis of alignment in the histogram and a much smaller correlation length (Figure 6b). The fan-shaped graph generated for each image illustrates the direction of alignment: roughly 80° for the aligned network and no major direction of alignment for the orthogonal network.

Electrical Transport Properties of Aligned and Orthogonal Networks of SWNTs.

To determine the effect of local SWNT orientation on macroscopic electrical transport, studies of the electrical transport properties of the two types of networks were performed. The resistance of 30 devices for each of the two patterns was measured in two directions: 0 and 90° with respect to the initial SWNT deposition direction (Figure 7). For example, when measuring the resistance at 0° for the aligned pattern, the electrical probes were aligned parallel to the SWNT deposition direction. On the contrary, for the measurement at 90°, the probes were aligned orthogonal to the deposit direction.

Aligned Pattern. For the aligned pattern, I/V curves displayed a remarkable anisotropy; conducting in one direction, but not the other. Figure 7a shows typical spectra for the aligned pattern measured in the direction orthogonal to the SWNT alignment (90°). When measured across the axis of alignment of the SWNTs, infinite resistance was observed. This is due to the lack of macroscopic electrical pathways in this direction.

The same sample shows a remarkably different response when measured in the orthogonal direction (0°). It exhibited Ohmic behavior over the range ±1 V and a resistance of 2.81 $\times$ 10^7 Ω (Figure 7b). This anisotropy in electrical response is a direct indication that the alignment direction of the SWNT deposition cycles has a strong effect on the macroscopic electrical properties of these 2D networks. Figure 8 represents resistance measurements for 30 devices with the aligned pattern. Although the $R = 3.47 \times 10^7$ Ω in the 0° direction, these devices had infinite R in the 90° direction.

Orthogonal Pattern. The resistance was measured for the orthogonal pattern devices in both the 90 and 0°
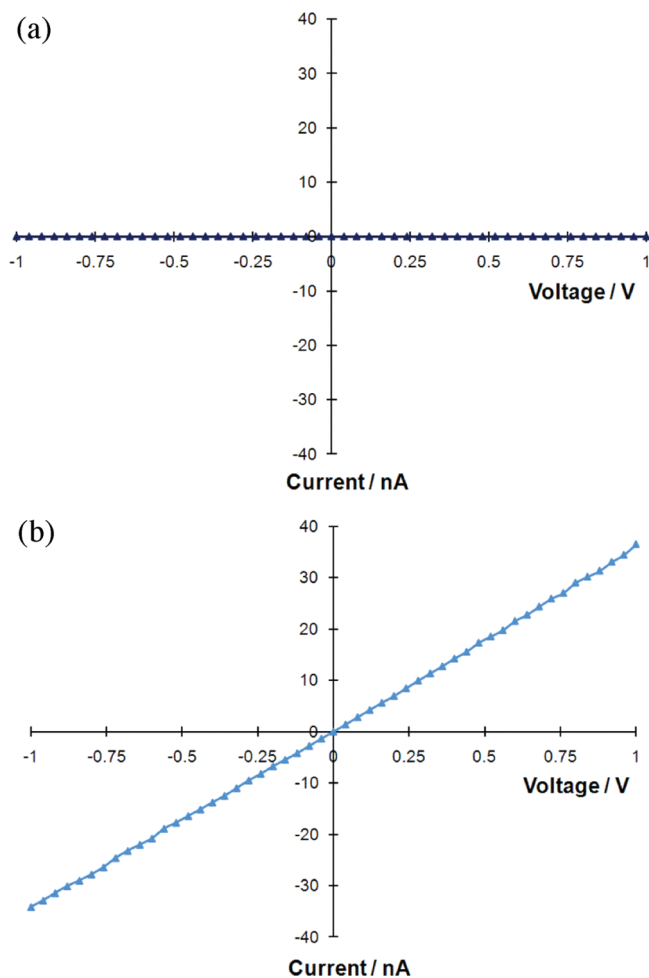
(a)

(b)

FIGURE 7. *I/V* curves typical of the macroscopic conductivity observed for the "aligned" pattern: (a) when measured in the 90° direction with respect to the initial SWNT alignment, this device has infinite resistance; (b) when measured in the 0° direction along with the initial SWNT alignment, this device has the resistance of 2.81 $\times$ 10^7 Ω.
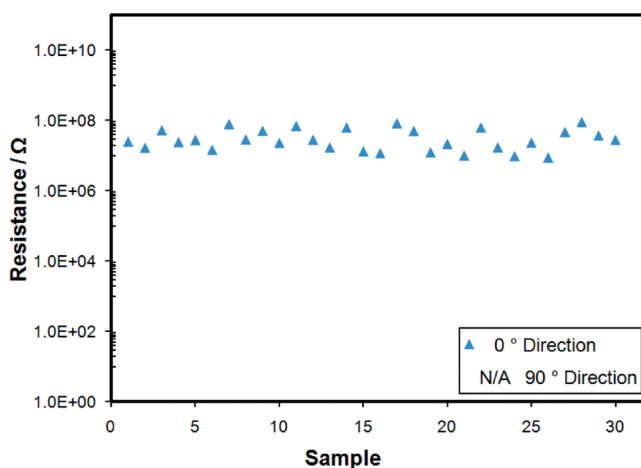
FIGURE 8. Macroscopic resistance of networks of "aligned" SWNTs. The average resistance (R_{ave}) for the 0° direction is 3.47 $\times$ 10^7 Ω; R_{ave} for the 90° direction is infinite.

directions with respect to the initial SWNTs deposition direction. The anisotropy observed for the aligned patterns was not observed. The average R for 30 different devices
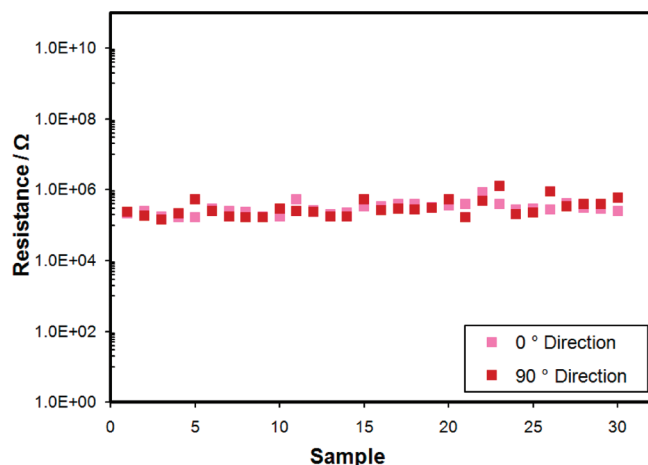
FIGURE 9. Resistance measurements of 30 devices for the "orthogonal" pattern. R_{ave} for the 0° direction is 3.08×10^5 Ω; R_{ave} for the 90° direction is 3.39×10^5 Ω.

(a)

(b)

FIGURE 10. I/V curves typical of the macroscopic conductivity observed for the "Orthogonal" pattern: (a) when measured in the 90° direction with respect to initial SWNT alignment, the resistance of this device is 3.27×10^5 Ω; (b) when measured in the 0° direction along with the initial SWNT alignment, this device has a resistance of 3.39×10^5 Ω.

for measurements in the 90° direction is 3.39×10^5 Ω (Figure 9). For the same devices measured in the 0° direction, the resistance is 3.08×10^5 Ω. Overall, there is much greater conformity in R for the orthogonal devices than for the aligned devices as the deposition method has the effect of creating a macroscopic deposit with a similar distribution of electrical pathways in both directions. For all measurements, the I/V curves showed Ohmic behavior. Figure 10a shows typical I/V responses for the orthogonal pattern measured in the 90° direction. The R for this I/V curve is 3.27×10^5 Ω. A similar response was observed for the 0° direction, with a resistance of 3.39×10^5 Ω (Figure 10b).

Aligned vs Orthogonal Pattern. Measuring each deposit in two directions yields information about how the macroscopic electronic transport varies with respect to the orientation of the SWNTs in the network, as controlled by the laminar flow deposition process. I/V curves for the two types of macroscopic networks showed a strong dependence of the macroscopic electrical conductivity on the local alignment of the SWNTs in the network. For measuring the overall resistance for both type of patterns, both types of devices displayed Ohmic behavior for source-drain voltages between −1 and +1 V in the 0° direction (Figures 7b and 10b). However, the "orthogonal" structures yielded a resistance of roughly 2 orders of magnitude less 3.39×10^5 Ω vs $R = 2.81 \times 10^7$ Ω. This difference in electronic transport indicates that although small scale devices would benefit from the higher current drive provided by highly aligned SWNTs, "orthogonal" nanostructures are a more efficient method of forming macroscopic conductive thin films than percolative networks composes of aligned SWNTs.

For the "aligned" pattern, when the electrical resistance was measured parallel to the direction of SWNT deposition, the average resistance was 2.81×10^7 Ω. However, if the measurement direction was rotated by 90° with respect to the alignment direction of the SWNTs, the infinite resistance was observed. This can be attributed to the formation of only short-range electrical pathways when the conducting wires are aligned in one direction (90°). Because of the high aspect
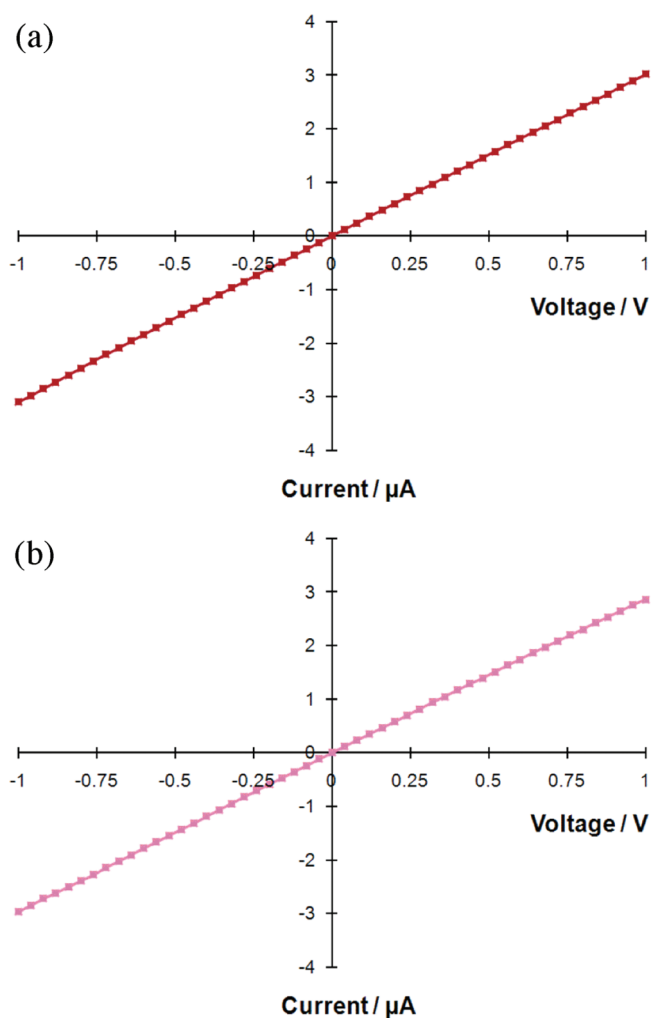
ratio of the SWNTs (their dimensions are approximately 1 nm × 1.2 μm), they are less likely to come into contact with one another in a deposit of aligned SWNTs, resulting in fewer electrical contacts and greater resistance over the macroscopic scale.

In contrast, there is much greater consistency in the resistance measurements for the "orthogonal" networks. The resistance in both directions varied comparatively little, from an average of 3.27×10^5 to 3.39×10^5 Ω for measurements at 0 and 90°, respectively. The observation of similar macroscopic resistances for both directions indicates a similar number of electrical pathways in both directions for the "orthogonal" networks. Overall, the "aligned" pattern shows significant variation in macroscopic resistance, limiting its applications to small area electronic materials where high current drive is needed, whereas the "orthogonal" pattern has slightly lower resistance and proves to be a more reproducible material, useful for large area electrical materials. Because reproducible densities of SWNTs are deposited in each deposition cycle and Ohmic behavior

ACS **APPLIED** **MATERIALS** **& INTERFACES**

ARTICLE

was observed for these networks, the macroscopic conduction observed was a linear function of the number of inter-SWNT junctions, with minimal influence from Schottky barriers or metal-SWNT contact resistance.

It is notable that both types of samples exhibited high resistance. This is due in part to the low densities of SWNTs used, contact resistance between SWNTs, and the presence of Schottky barriers at connections between metallic and semiconductive SWNTs. Possible routes to addressing the low conductivity of these networks include the use of higher-density networks, selective deposition of a thin-layer of a conductive polymer on the SWNTs (46), nitric acid treatments (47), use of suspensions of SWNTs that have been enriched in semiconductive or metallic SWNTs (48), or a postdeposition spray-coating of a layer of SWNTs (49).

CONCLUSION

The electrical resistance of a device composed of "aligned" or "orthogonal" nanostructures was measured in two directions; parallel (0°) to the direction of alignment of the SWNTs and then perpendicular (90°) to it. Anisotropic electronic properties were observed in "aligned" networks, while "orthogonal" SWNT thin films exhibited greater isotropy. These measurements indicate that the formation of "orthogonal" nanostructures presents a route to the reproducible formation of transparent electrical materials, with the lowest possible loading of SWNT material. "Orthogonal" nanostructures consistently displayed lower resistance and less variability in resistance measurements between devices, making them an ideal candidate for applications that involve formation of macroscopic conductive thin films from nanoscale conductors.

In the short term, this method of formation of orthogonal nanostructures will be useful in electronic applications that require macroscopic, conductive thin-film networks. "Orthogonal" nanostructures enable formation of conductive thin films with the lowest possible loading of SWNT material. Additionally, controlled formation of nanostructures results in macroscopic materials with tunable and reproducible properties. Therefore, these results indicate a significant step toward the goal of incorporation of nanoscale materials to functional electronic device structures, as this deposition method can be combined with micropatterned silane layers to obtain a high degree of positional control. Another major advantage of this route to SWNT network formation is that the density of SWNTs is controlled easily by varying solution composition and/or deposition cycles.

REFERENCES AND NOTES

(1) Dai, H. J. *Surf. Sci.* **2002**, *500*, 218.
(2) Tan, E. P. S.; Lim, C. T. *Compos. Sci. Technol.* **2006**, *66*, 1102.
(3) Bhattacharyya, S.; Salvetat, J. P.; Saboungi, M. L. Appl. Phys. Lett. 2006, 88.
(4) Strano, M. S.; Dyke, C. A.; Usrey, M. L.; Barone, P. W.; Allen, M. J.; Shan, H. W.; Kittrell, C.; Hauge, R. H.; Tour, J. M.; Smalley, R. E. *Science* **2003**, *301*, 1519.
(5) Haremza, J. M.; Hahn, M. A.; Krauss, T. D. *Nano Lett.* **2002**, *2*, 1253.
(6) Bradley, K.; Gabriel, J. C. P.; Gruner, G. *Nano Lett.* **2003**, *3*, 1353.
(7) Zhang, Y.; Deng, S. Z.; Xu, N. S.; Chen, J. *J. Vac. Sci. Technol., B* **2008**, *26*, 1033.
(8) Takeda, S.; Nakamura, M.; Subagyo, A.; Ishii, A.; Sueoka, K.; Mukasa, K. *Sens. Actuators, B* **2008**, *132*, 9.
(9) Shiau, S. H.; Liu, C. W.; Gau, C.; Dai, B. T. *Nanotechnology* **2008**, *19*, 105303.
(10) Chaste, J.; Lechner, L.; Morfin, P.; Feve, G.; Kontos, T.; Berroir, J. M.; Glattli, D. C.; Happy, H.; Hakonen, P.; Placais, B. *Nano Lett.* **2008**, *8*, 525.
(11) Li, H.; Yin, W. Y.; Banerjee, K.; Mao, J. F. *IEEE Trans. Electron Devices* **2008**, *55*, 1328.
(12) Zhou, Y.; Sreekala, S.; Ajayan, P. M.; Nayak, S. K. *J. Phys.: Condens. Matter* **2008**, *20*, 095209.
(13) Lan, C.; Zakharov, D. N.; Reifenberger, R. G. *Appl. Phys. Lett.* **2008**, *92*, 213112.
(14) Coiffic, J. C.; Fayolle, M.; Faucherand, P.; Levis, M.; Le Poche, H.; Dijon, J.; Maitrejean, S. *Phys. Status Solidi A* **2008**, *205*, 1399.
(15) Kang, S. J.; Kocabas, C.; Kim, H. S.; Cao, O.; Meitl, M. A.; Khang, D. Y.; Rogers, J. A. *Nano Lett.* **2007**, *7*, 3343.
(16) Zhou, Y. X.; Hu, L. B.; Gruner, G. *Appl. Phys. Lett.* **2006**, *88*, 123109.
(17) Novak, J. P.; Lay, M. D.; Perkins, F. K.; Snow, E. S. *Solid-State Electron.* **2004**, *48*, 1753.
(18) Vairavapandian, D.; Vichchulada, P.; Lay, M. D. *Anal. Chim. Acta* **2008**, *626*, 119.
(19) Wang, J.; Timchalk, C.; Lin, Y. H. *Environ. Sci. Technol.* **2008**, *42*, 2688.
(20) Ruffini, G.; Dunne, S.; Fuentemilla, L.; Grau, C.; Farres, E.; Marco-Pallares, J.; Watts, P. C. P.; Silva, S. R. P. *Sens. Actuators, A* **2008**, *144*, 275.
(21) Gan, T.; Li, K.; Wu, K. B. *Sens. Actuators, B* **2008**, *132*, 134.
(22) Sivaramakrishnana, S.; Rajamani, R.; Smith, C. S.; McGee, K. A.; Mann, K. R.; Yamashita, N. *Sens. Actuators, B* **2008**, *132*, 296.
(23) Lee, C. Y.; Sharma, R.; Radadia, A. D.; Masel, R. I.; Strano, M. S. *Angew. Chem., Int. Ed.* **2008**, *47*, 5018.
(24) Kumar, M. K.; Reddy, A. L. M.; Ramaprabhu, S. *Sens. Actuators, B* **2008**, *130*, 653.
(25) Gong, J. W.; Sun, J. R.; Chen, Q. F. *Sens. Actuators, B* **2008**, *130*, 829.
(26) Artukovic, E.; Kaempgen, M.; Hecht, D. S.; Roth, S.; Gruner, G. *Nano Lett.* **2005**, *5*, 757.
(27) Cattanach, K.; Kulkarni, R. D.; Kozlov, M.; Manohar, S. K. *Nanotechnology* **2006**, *17*, 4123.
(28) Nomura, K.; Ohta, H.; Takagi, A.; Kamiya, T.; Hirano, M.; Hosono, H. *Nature* **2004**, *432*, 488.
(29) Parikh, K.; Cattanach, K.; Rao, R.; Suh, D. S.; Wu, A. M.; Manohar, S. K. *Sens. Actuators, B* **2006**, *113*, 55.
(30) Joselevich, E.; Dai, H. J.; Liu, J.; Hata, K.; Windle, A. H. *In Carbon Nanotubes* **2008**, *111*, 101.
(31) LeMieux, M. C.; Roberts, M.; Barman, S.; Jin, Y. W.; Kim, J. M.; Bao, Z. N. *Science* **2008**, *321*, 101.
(32) Kocabas, C.; Pimparkar, N.; Yesilyurt, O.; Kang, S. J.; Alam, M. A.; Rogers, J. A. *Nano Lett.* **2007**, *7*, 1195.
(33) Vichchulada, P.; Zhang, Q.; Lay, M. D. *Analyst* **2007**, *132*, 719.
(34) Vichchulada, P.; Lipscomb, L. D.; Zhang, Q.; Lay, M. D. *J. Nanosci. Nanotechnol.* **2009**, *9*, 2189.
(35) Lay, M. D.; Novak, J. P.; Snow, E. S. *Nano Lett.* **2004**, *4*, 603.
(36) Vichchulada, P.; Shim, J.; Lay Marcus, D. *J. Phys. Chem. C* **2008**, *112*, 19186.
(37) Zhang, Q.; Vichchulada, P.; Lay, M. D. *J. Mater. Sci.* **2008**, *44*, 1206.
(38) Jeong, H.; Gweon, H. M.; Kwon, B. J.; Ahn, Y. H.; Park, J. Y. *Nanotechnology* **2009**, *20*, 345202.
(39) Trionfi, A.; Scrymgeour, D. A.; Hsu, J. W. P.; Arlen, M. J.; Tomlin, D.; Jacobs, J. D.; Wang, D. H.; Tan, L. S.; Vaia, R. A. *J. Appl. Phys.* **2008**, *104*, 083708.
(40) Lian, Y. F.; Maeda, Y.; Wakahara, T.; Akasaka, T.; Kazaoui, S.; Minami, N.; Choi, N.; Tokumoto, H. *J. Phys. Chem. B* **2003**, *107*, 12082.
(41) Maeda, Y.; Kimura, S.; Kanda, M.; Hirashima, Y.; Hasegawa, T.; Wakahara, T.; Lian, Y. F.; Nakahodo, T.; Tsuchiya, T.; Akasaka, T.; Lu, J.; Zhang, X. W.; Gao, Z. X.; Yu, Y. P.; Nagase, S.; Kazaoui, S.; Minami, N.; Shimizu, T.; Tokumoto, H.; Saito, R. *J. Am. Chem. Soc.* **2005**, *127*, 10287.

(42) Dresselhaus, M. S.; Dresselhaus, G.; Jorio, A.; Souza, A. G.; Saito, R. *Carbon* **2002**, *40*, 2043.

(43) Shin, H. J.; Kim, S. M.; Yoon, S. M.; Benayad, A.; Kim, K. K.; Kim, S. J.; Park, H. K.; Choi, J. Y.; Lee, Y. H. *J. Am. Chem. Soc.* **2008**, *130*, 2062.

(44) Brown, S. D. M.; Corio, P.; Marucci, A.; Pimenta, M. A.; Dresselhaus, M. S.; Dresselhaus, G. *Phys. Rev. B* **2000**, *61*, 7734.

(45) Corio, P.; Brown, S. D. M.; Marucci, A.; Pimenta, M. A.; Kneipp, K.; Dresselhaus, G.; Dresselhaus, M. S. *Phys. Rev. B* **2000**, *61*, 13202.

(46) Ma, Y. F.; Cheung, W.; Wei, D. G.; Bogozi, A.; Chiu, P. L.; Wang, L.; Pontoriero, F.; Mendelsohn, R.; He, H. X. *ACS Nano* **2008**, *2*, 1197.

(47) Nirmalraj, P. N.; Lyons, P. E.; De, S.; Coleman, J. N.; Boland, J. J. *Nano Lett.* **2009**, *9*, 3890.

(48) Qiu, H. X.; Maeda, Y.; Akasaka, T. *J. Am. Chem. Soc.* **2009**, *131*, 16529.

(49) Song, Y. I.; Yang, C. M.; Kim, D. Y.; Kanoh, H.; Kaneko, K. *J. Colloid Interface Sci.* **2008**, *318*, 365.

AM900706P